Studies on the Thermal Degradation of Poly (*p*-phenylene benzobisoxazole)

K. Tamargo-Martínez, S. Villar-Rodil,* J. I. Paredes, A. Martínez-Alonso, and J. M. D. Tascón

Instituto Nacional del Carbón, CSIC, Apartado 73, 33080 Oviedo, Spain

Received May 9, 2003. Revised Manuscript Received July 16, 2003

Thermal decomposition of poly(*p*-phenylene benzobisoxazole) (PBO) has been studied between room temperature and 1123 K. Two types of material (regular and high-modulus) were studied, which yielded almost equivalent results. Thermogravimetry and differential thermal analysis allowed establishing the main stages of the pyrolytic degradation of the material. On the basis of the thermal analysis results, samples were decomposed at several controlled temperatures and characterized by elemental analysis, infrared spectroscopy, X-ray diffraction, atomic force microscopy, and scanning tunneling microscopy. At temperatures below 933 K the polymer retains its original conformation and becomes stabilized by enhancement of its crystallinity. The decomposition takes place in a single step and the main changes occur within a very narrow temperature interval (983−993 K). Formation of polyaramides as intermediates in the decomposition process was detected. These amide bonds subsequently degrade by homolytic breaking, yielding nitriles. The final carbonaceous residue is rich in nitrogen and retains a certain degree of anisotropy, a fact that was explained by the conservation of crystallinity at an intermediate decomposition stage.

Introduction

Because of their outstanding physical and mechanical properties, rigid-rod polymers are attractive materials for use in high-performance structural applications, including aircraft components or fire protection garments, as constituents of both traditional (e.g., fiber-reinforced) and molecular composites.[1] Among rigid-rod polymers, poly(*p*-phenylene benzobisoxazole), known as PBO (Scheme 1), has been the focus of much research attention, not only from an experimental point of view[2−9] but also from a theoretical perspective.[10,11] The synthesis of PBO involves polymerization of 4,6-diamino-1,3-benzenediol with an intermediate obtained from reaction of poly(phosphoric acid) and terephthaloyl dichloride. A solution of the resultant PBO polymer in a strong acid is then dry-jet wet spun, thus producing fibers with a high degree of molecular orientation, and, accordingly, remarkable Young's modulus and tensile strength.[5]

Scheme 1. Chemical Structure of PBO

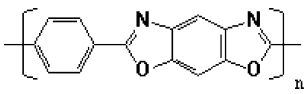

In addition to its advantageous mechanical characteristics, PBO displays a good chemical resistance and excellent thermal stability.[1] The latter attribute makes this polymer particularly suitable for high-temperature applications. Although the origin of such behavior can be ultimately traced to the high conjugation and rigidity of its constituent molecules, a detailed understanding of the thermal degradation process of PBO becomes essential if its application in the mentioned fields is to be fully realized. In the past, the thermal degradation of PBO has been studied by means of indirect methods, i.e., through the analysis of the compounds evolved during pyrolysis, which provided valuable information on the chemistry of the process.[12−16] The techniques employed for this purpose were mainly thermal analysis, mass spectrometry, and gas chromatography. However, direct information on the progressive changes

* Corresponding author. Telephone: (+34) 985 11 90 90. Fax: (+34) 985 29 76 62. E-mail: silviam@incar.csic.es.

(1) Jiang, H.; Adams, W. W.; Eby, R. K. In *Handbook of Fiber Science and Technology*; Lewin, M., Perston, J., Eds.; Marcel Dekker: New York, 1996; Vol. III, Chapter 2.
(2) Krause, S. J.; Haddock, T. B.; Vezie, D. L.; Lenhert, P. G.; Hwang, W.-F.; Price, G. E.; Helminiak, T. E.; O'Brien, J. F.; Adams, W. W. *Polymer* **1988**, *29*, 1354.
(3) Martin, D. C.; Thomas, E. L. *Macromolecules* **1991**, *24*, 2450.
(4) Connolly, J. W.; Dudis, D. S.; Kumar, S.; Gelbaum, L. T.; Venkatasubramanian, N. *Chem. Mater.* **1996**, *8*, 54.
(5) Kitagawa, T.; Murase, H.; Yabuki, K. *J. Polym. Sci., Part B: Polym. Phys.* **1998**, *36*, 39.
(6) Kitagawa, T.; Yabuki, K.; Young, R. J. *Polymer* **2001**, *42*, 2101.
(7) Takahashi, Y. *J. Polym. Sci., Part B: Polym. Phys.* **2001**, *39*, 1791.
(8) Alam, M. M.; Jenekhe, S. A. *Chem. Mater.* **2002**, *14*, 4775.
(9) Ran, S.; Burger, C.; Fang, D.; Zong, X.; Cruz, S.; Chu, B.; Hsiao, B. S.; Bubeck, R. A.; Yabuki, K.; Teramoto, Y.; Martin, D. C.; Johnson, M. A.; Cunniff, P. M. *Macromolecules* **2002**, *35*, 433.
(10) Martin, D. C. *Macromolecules* **1992**, *25*, 5171.
(11) Jones, M.-C. G.; Martin, D. C. *Macromolecules* **1995**, *28*, 6161.
(12) Voloshchuk, K. A.; Popovic, I.; Martinov, S. V.; Donskikh, A. I.; Tseitlin, G. M.; Velickovic, J. *J. Therm. Anal.* **1993**, *40*, 773.
(13) Kuroki, T.; Tanaka, Y.; Hokudoh, T.; Yabuki, K. *J. Appl. Polym. Sci.* **1997**, *65*, 1031.
(14) So, Y.-H.; Froelicher, S. W.; Kaliszewski, B.; DeCaire, R. *Macromolecules* **1999**, *32*, 6565.
(15) Wu, Z.; Li, F.; Huang, L.; Shi, Y.; Jin, X.; Fang, S.; Chuang, K.; Lyon, R. E.; Harris, F. W.; Cheng, S. Z. D. *J. Therm. Anal. Calorim.* **2000**, *59*, 361.
(16) Bourbigot, S.; Flambard, X.; Duquesne, S. *Polym. Int.* **2001**, *50*, 157.

10.1021/cm034336u CCC: $25.00
Published on Web 08/30/2003

undergone by the solid material upon heat treatment is not currently available.

Consequently, the present work was aimed at documenting by direct means the chemical and morphological transformations of PBO upon pyrolysis. To this end, two different techniques that provide complementary information were mainly employed at several different stages of the thermal degradation: (i) diffuse reflectance infrared Fourier transform spectroscopy (DRIFTS), which showed evidence of the chemical transformations of the polymer during the degradation process, and (ii) scanning probe microscopies (SPM), specifically atomic force and scanning tunneling microscopies (AFM/STM), which enabled the concomitant morphological changes to be tracked on the nanometer scale. Thermal analysis (TGA/DTG/DTA) was used to identify the different stages of the degradation. Moreover, additional information was provided by elemental analysis and X-ray diffraction measurements of the samples. Infrared spectroscopy has been previously employed to study the degradation (thermal, hydrolytic, etc.) of other polymeric materials.[17−19] By contrast, the use of SPM to visualize the morphological changes of polymers during their degradation (particularly, thermal degradation) has been much less common,[18−20] even though it is widely employed to investigate other processes on these materials, such as annealing or different types of surface treatments.[21−24] In the specific case of PBO this work presents, to the best of our knowledge, the first SPM images of the mentioned polymer, either virgin or after any sort of treatment.

Experimental Section

PBO fibers were supplied by Toyobo Ltd. under the trademark Zylon. Two types of PBO fibers, a regular type (AS) and a high modulus one (HM), were used as starting materials in this study. AS stands for as-spun fiber whereas HM fiber is produced from AS fiber by heat treatment (several seconds to a few minutes, 923 K temperature and 0.7 GPa tension).[6]

Simultaneous thermogravimetry (TG)/differential thermal analysis (DTA) experiments were carried out in a Stanton-Redcroft STA-1500 thermogravimetric analyzer provided with a Plus-V software. As-received fibers, without drying, were used in all thermal treatments. Samples (∼20 mg) were placed in Pt crucibles of 5-mm diam. and 5-mm height. An argon (99.9990% pure by volume) constant flow of 50 cm^3 min^{-1} at atmospheric pressure was used. The reference material for DTA measurements was α-alumina. Temperatures were measured with Pt/Rh thermocouples placed at the bottom of the Pt crucibles, in contact with them. Samples pyrolyzed to various carefully controlled extents were prepared in the same thermobalance under the same conditions, by heating at 10 K min^{-1} to different selected temperatures and effectively stopping the process by rapid cooling to room temperature. These samples were considered to be representative of the different decomposition stages undergone by the material.

Elemental analyses of the starting material and the heat-treated samples were carried out in a LECO CHNS-932 microanalysis apparatus with a LECO VTF-900 accessory for oxygen.

DRIFTS spectra of all samples were obtained in a Nicolet Magna IR560 spectrometer using a high-sensitivity MCT/A detector. The spectra shown are the result of coadding 200 interferograms obtained at a resolution of 4 cm^{-1}.

X-ray diffraction measurements were performed in a Siemens D5000 diffractometer using Cu Kα radiation ($\lambda = 1.5405$ nm), with a step size of 0.015° and a step time of 3 s. For obtaining meridional diffractograms, fiber bundles were pulled through a glass column and the excess fiber material at the column end was carefully cut to obtain a very flat surface. The fibers packed in this way were attached vertically so that the flat surface was the plane onto which the incident X-ray beam diffracted. This method could not be satisfactorily implemented for heat-treated samples, in which case a parallel arrangement of fibers was difficult to obtain. Average crystal sizes for axial and lateral directions in the case of the polymer and along the *c* axis in the case of the final carbonaceous material were estimated from the measured widths of the diffraction peaks with the use of Scherrer's formula.

SPM investigations were conducted to follow the morphological evolution of the polymer with heat treatment temperature up to the attainment of the final fibrous carbon residue. To this end, a Nanoscope Multimode IIIa apparatus, from Digital Instruments, was employed in air at room temperature. Thin, sparse bundles of the fresh and heat-treated PBO fibers were mounted onto metallic SPM sample holders making use of double-sided carbon adhesive tape. Special care was required to avoid the presence of fibers sticking out from the sample surface, which could touch the SPM probe at points other than the very tip apex and invalidate the measurement. Most of the SPM observations were carried out by means of AFM in the tapping mode of operation, which has previously shown to provide an accurate description of the morphological changes undergone by other polymers during their thermal degradation.[19] However, to further support the AFM observations, STM was also performed on the pyrolyzed samples whenever possible, i.e., on those specimens which displayed a conductivity large enough for STM to be practicable. Such condition was fulfilled only at late stages of the degradation process.

For the tapping mode AFM studies, rectangular silicon cantilevers (Digital Instruments) with spring constants between 20 and 100 N m^{-1} and nominal tip radii of curvature of 5−10 nm (as specified by the manufacturer) were employed. Their typical resonance frequencies were around 250 kHz. Imaging was performed in the intermittent contact regime (as determined from phase−distance curves)[25] with free and setpoint amplitudes of about 100 and 90 nm, respectively. These parameters allowed the sample surface topography to be tracked accurately and reproducibly under light tapping forces, thus reducing sample disturbance to a minimum. Concerning the STM observations, mechanically prepared Pt/Ir (80/20) tips were utilized. Imaging was accomplished in constant current mode (variable height) so as to obtain topographical information of the sample surface. Typical tunneling conditions were 600 mV and 0.5 nA for the bias voltage and tunneling current, respectively, although it was checked that such parameters could be modified considerably without noticeable changes in the corresponding images. In general, to ensure that the features detected in the images were reproducible and representative of the analyzed samples, several different and previously unused probes were employed for both AFM and STM. Moreover, for each PBO sample, many different fibers were investigated and many different areas on each fiber were surveyed.

Results

Thermal Analysis. Figure 1 shows TG, DTG, and DTA graphs for HM and AS Zylon fibers. HM Zylon

(17) Dubois, M.; Naji, A.; Buisson, J. P.; Humbert, B.; Grivei, E.; Billaud, D. *Carbon* **2000**, *38*, 1411.
(18) Sukpirom, S.; Lerner, M. M. *Chem. Mater.* **2001**, *13*, 2179.
(19) Villar-Rodil, S.; Paredes, J. I.; Martínez-Alonso, A.; Tascón, J. M. D. *Chem. Mater.* **2001**, *13*, 4297.
(20) Murase, T.; Iwata, T.; Doi, Y. *Macromolecules* **2001**, *34*, 5848.
(21) Ton-That, C.; Teare, D. O. H.; Campbell, P. A.; Bradley, R. H. *Surf. Sci.* **1999**, 433−435, 278.
(22) Mahlberg, R.; Niemi, H. E.-M.; Denes, F. S.; Rowell, R. M. *Langmuir* **1999**, *15*, 2985.
(23) Ton-That, C.; Teare, D. H. O.; Bradley, R. H. *Chem. Mater.* **2000**, *12*, 2106.
(24) Reiter, G.; Castelein, G.; Sommer, J.-U.; Röttele, A.; Thurn-Albrecht, T. *Phys. Rev. Lett.* **2001**, *87*, 226101.
(25) James, P. J.; Antognozzi, M.; Tamayo, J.; McMaster, T. J.; Newton, J. M.; Miles, M. J. *Langmuir* **2001**, *17*, 349.

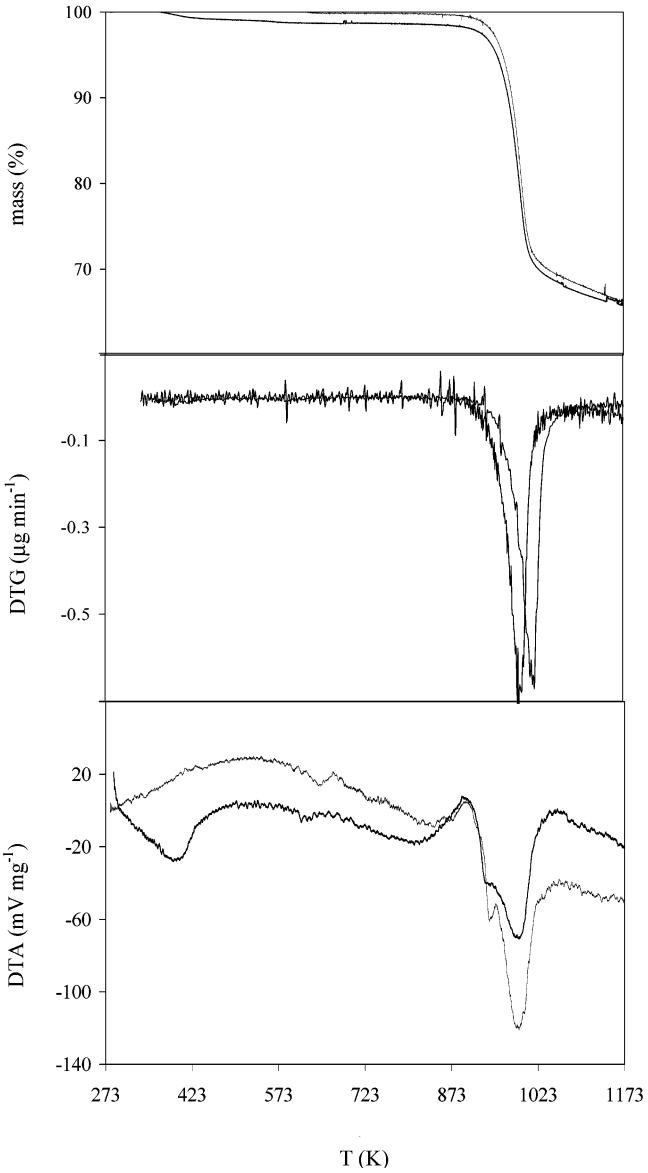

Figure 1. TG, DTG, and DTA curves for Zylon AS (black) and Zylon HM (grey) pyrolysis under argon with a heating rate of 10 K min^{-1}.

fibers show no moisture release, whereas AS Zylon fibers exhibit a ∼1% water loss from 373 K on, accompanied by a DTA endothermal effect centered at 400 K. In the DTA curves for both types of fibers, a barely appreciable but reproducible endothermal effect appears at around 600−650 K (this is observed systematically in this work as well as in other studies).[26] A weak exothermal effect with maximum at 900 K, starting at around 800 K for Zylon AS and 850 K for Zylon HM also appears.

Both fibers show an outstanding thermal stability, as there are no appreciable mass changes until 840 K; the mass loss becoming significant above 933 K. The main mass loss takes place in a single step from this temperature up to 1050 K, being especially prominent between 973 and 993 K. This degradation step gives rise to a DTG peak with a minimum at 1020 K (for Zylon AS) and is accompanied by an endothermal effect in the DTA curve, consisting of two peaks with minima centered at 945 and 993 K, respectively. From 1050 K on, the mass loss rate is lower and fairly constant up to 1173 K, where the carbonization yield is 66 wt %. The only significant difference between the TG results of the two fibers, HM and AS, is the moisture release. However, recalculating the mass percent for Zylon AS on a dry basis, the TG curves overlap to ± 0.5%.

On the basis of these thermal analyses, several temperatures were selected as representative of the different steps of the degradation process. Particular emphasis was placed on a range of temperatures around 990 K, where the main mass loss takes place, and, consequently, the major changes are expected to occur. Batches were prepared by stopping the process at such temperatures by quickly cooling the pyrolyzed sample to room temperature.

Elemental Analysis. Table 1 shows the elemental analyses on a dry basis of Zylon AS samples heat-treated to different temperatures. Zylon HM samples yielded very similar results and they have been omitted to avoid repetition. The starting material does not contain inorganic impurities in detectable quantity as the analyzed elements (C, H, O, N) sum 100 wt. % within the experimental error. The sample gradually increases its content of C, as expected in any carbonization process, while its atomic percentage of hydrogen decreases. As for the other heteroatoms, oxygen and nitrogen, they are in 1:1 atomic ratio in the starting material, as expected from the chemical formula of the polymer, and their atomic percents remain similar up to 973 K. From this temperature on, oxygen is lost to a greater extent than nitrogen, with oxygen and nitrogen being in 1:2 atomic ratio at 1073 K, as deduced from Table 1. It must be noted that the nitrogen content of the final carbonized fiber is outstandingly high (∼10wt % at 1073 K), while hydrogen is barely present.

Infrared Spectroscopy Measurements. The DRIFTS results presented henceforth were found to be equivalent for the two types of fibers (AS and HM). Although only the spectra for Zylon AS are shown (Figure 2), they will refer to both of them. The spectrum of fresh Zylon AS can be seen in Figure 2a. As already indicated, the base polymer for this fiber is PBO. According to this chemical structure, the following band assignments can be made: a wide band centered at 3430 cm^{-1}, N−H and O−H stretching vibrations of amine and hydroxyl end groups; 3097 and 3069 cm^{-1}, C−H stretching vibrations of the benzene ring between the two oxazole rings, the highest wavenumber corresponding to the C−H closer to oxygen; 3040 cm^{-1}, C−H stretching vibrations of the phenyl ring; 1618 cm^{-1}, C═C stretching vibrations of aromatic rings and C═N bonds in cyclic compounds; 1579 and 1497 cm^{-1}, skeletal vibrations of the conjugated system; 1329 and 1309 cm^{-1}, C−N stretching; 1278 cm^{-1}, C−C stretching of the carbons linking the heterocycle and the phenyl ring; 1148 and 1060 cm^{-1}, asymmetric stretching vibration of an unsaturated cyclic ether; 1116 and 1012 cm^{-1}, C−H in-plane deformations in substituted aromatic rings; 926 and 916 cm^{-1}, symmetric C−O−C stretching vibration of a cyclic ether; and 865, 853, 824, and 708 cm^{-1}, out-of-plane C−H vibrations of aromatic rings. The fact that

(26) Bourbigot, S.; Flambard, X.; Poutch, F., *Polym. Degrad. Stabil.* **2001**, *74*, 283−290.

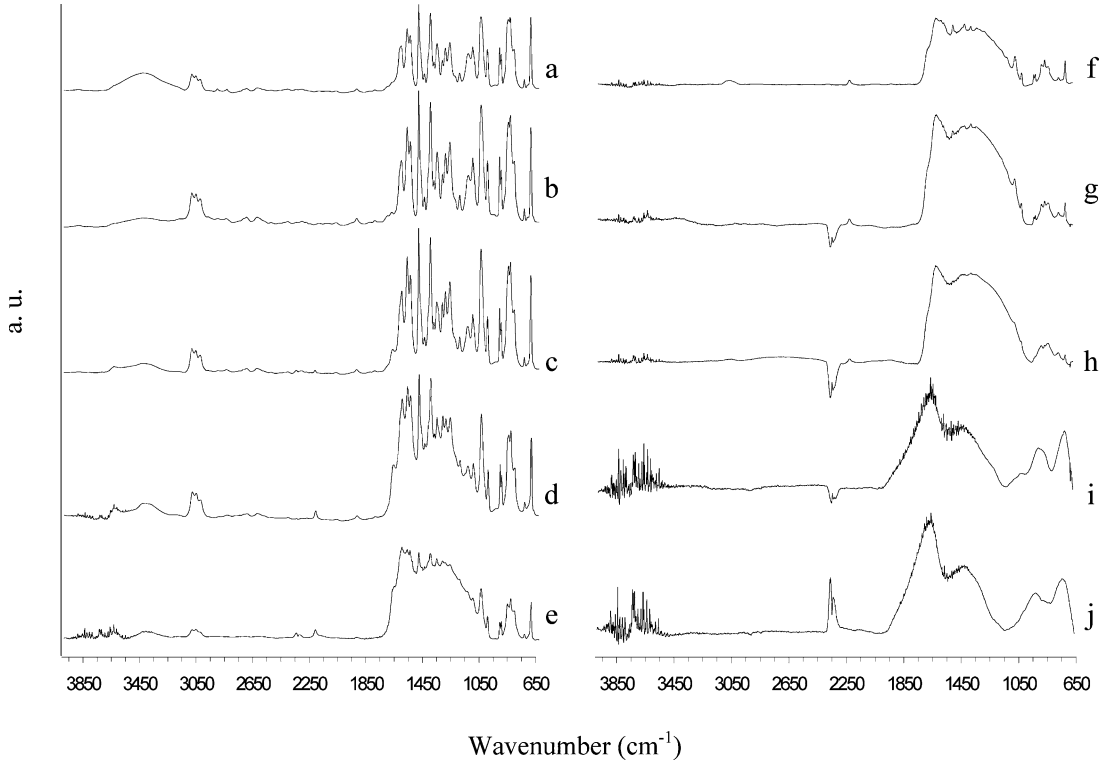

Figure 2. FTIR spectra of fresh Zylon AS (a) and its solid decomposition products at 873 (b), 933 (c), 963 (d), 978 (e), 983 (f), 988 (g), 993 (h), 1073 K (i), and 1123 K (j).

Table 1. Chemical Analyses of Zylon AS, Fresh and Heat-treated to Various Temperatures

T (K)	C (wt %)	H (wt %)	O (wt %)	N (wt %)	C (atomic %)	H (atomic %)	O (atomic %)	N (atomic %)
293	71.42	2.54	14.46	12.20	56.12	26.88	8.86	8.14
953	72.83	2.46	13.51	10.63	59.99	24.15	8.35	7.51
973	75.81	0.20	11.46	11.90	78.15	2.46	8.87	10.52
993	81.86	0.19	6.45	11.40	82.90	2.29	4.90	9.90
1073	85.13	0.08	5.51	9.89	86.25	0.97	4.19	8.59

most of the peaks arise from the vibrational modes of the ring system makes it difficult to assign individual frequencies to particular vibrational modes.[27] The spectra for fresh Zylon AS (Figure 2a) and HM (not shown) are equivalent except for the fact that the amine and hydroxyl end groups are more significant in Zylon AS (compared to HM); i.e., the ratio of the intensity of this band to the other bands in the spectrum is higher in Zylon AS. The only appreciable change observed in the IR spectra until 873 K is the decrease in the intensity of the band ascribed to end groups in relation to the other bands (compare Figure 2a with 2b). This change is less appreciable for Zylon HM.

At 933 K (Figure 2c), the wide band centered at around 3400 cm^{-1} intensifies, accompanied by the appearance and growth of another one at 1686 cm^{-1}. These two bands are assigned to the stretching vibrations of a N−H bond and a C═O bond in an amide group, respectively. Amides could be originated by the transformation of an oxazole ring into an acyclic amide. This reorganization could take place without breaking of the polymeric backbone. Also at 933 K, an absorption band with a very weak intensity appears at 2220 cm^{-1}, which can be assigned to the stretching vibration of a C≡N bond in an aryl nitrile. The appearance of this group does imply a breaking of the polymeric backbone. Indeed, aryl nitriles were found as evolved products in the previous indirect studies performed on the degradation of PBO.[14] Aryl nitriles are also found as intermediates in the degradation of related high-strength polymers, such as polyaramides.[19,28] In fact, while the intensities of the nitrile bands increase from 933 K on, those of the bands ascribed to the bonds in the oxazole groups (1620 cm^{-1}, for C═N; 1328 and 1308 cm^{-1}, for C−N; 1148 cm^{-1}, for the ether) decrease until almost disappearing at 978 K (Figure 2e). Also the intensity of the band centered at 1278 cm^{-1}, which was assigned to the C−C bond between benzobisoxazole and phenyl groups, drops in this temperature range [particularly, between 963 (Figure 2d) and 978 K (Figure 2e)], as this bond breaks when nitriles are formed (nitriles are linked to the benzene ring in the original benzobisoxazole group).[14]

The nitrile band is no longer observed above 978 K (Figure 2e), as it decomposes, whereas the bands related to amide groups (1686 cm^{-1} or amide I band and 1557 cm^{-1} or amide II band) vanish between 978 and 988 K (Figure 2e to 2g). From 978 K onward, the bands assigned to vibration of aromatic hydrogens decrease in intensity, and two wide bands, typical for carbonized

(27) O'Sullivan, D. G. *J. Chem. Soc.* **1960**, 3278.

(28) Mosquera, M. E. G.; Jamond, M.; Martínez-Alonso, A.; Tascón, J. M. D. *Chem. Mater.* **1994**, *6*, 1918−1924.

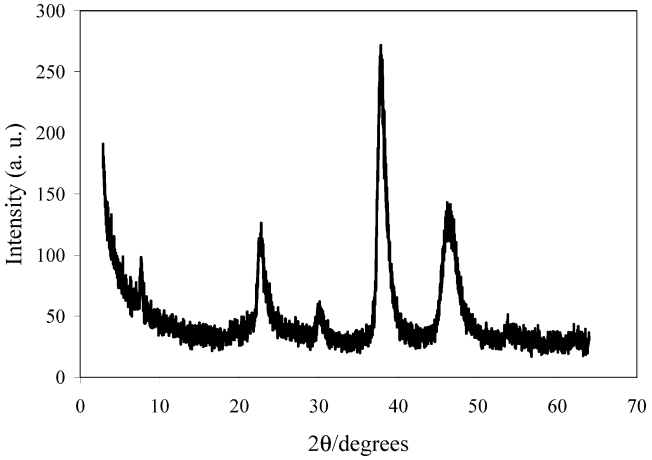

Figure 3. Meridional X-ray diffractogram of fresh Zylon AS.

materials,[19] appear around 1620 and 1400 cm^{-1}. The band at 1620 cm^{-1} can be ascribed to C═C skeletal vibrations in polynuclear aromatic hydrocarbons or aromatic compounds substituted by functional groups with heteroatoms. Probably both types of species are present in the product, giving rise to a mixed band. In any case, the observation of such band is an indication of the increasing aromaticity of the material as polycondensation reactions take place, which is in turn related to the increase in carbon content together with the decrease in hydrogen observed in the elemental analyses (Table 1). At 993 K (Figure 2h), only these two bands remain in the spectrum. Therefore, we conclude that the critical chemical changes take place in a narrow temperature range from 983 to 993 K, in which any sign of the bands related to the initial polymeric structure vanishes completely to bring in those typical of carbonized materials.

At 1073 K (Figure 2i), the band initially centered at 1620 cm^{-1} has widened and shifted to higher wavenumbers, being centered at 1689 cm^{-1} after heating at 1123 K (Figure 2j). This shift could be due to the appearance of lactone groups. This is not found in other related carbonized polymers[19,28] and could be connected with the noticeably high percentage of heteroatoms found in the elemental analyses of the pyrolyzed products.

X-ray Diffraction Measurements. Meridional and equatorial X-ray diffraction intensity profiles for Zylon AS are shown in Figures 3 and 4, respectively. Zylon HM profiles are not shown to avoid repetition. Whereas the meridional diffractogram is related to the order along the fiber axis, the equatorial reflection reveals the intermolecular arrangement between chains. Table 2 shows average crystal sizes for both axial and lateral directions calculated with the Scherrer's equation using the most intense diffraction peaks in each direction, which were assigned to (005) and (200) diffractions,[2] respectively.

The fresh HM sample shows higher values for average crystal sizes in both directions than the AS sample, which reveals the higher crystallinity of the HM sample. Indeed, the higher value of the crystal size in the axial direction obtained for HM fiber justifies its higher Young's modulus. The values obtained for lateral average crystal sizes match well with those found by Kitagawa et al.[5] An increase of the average crystal size upon thermal treatment is observed for both types of

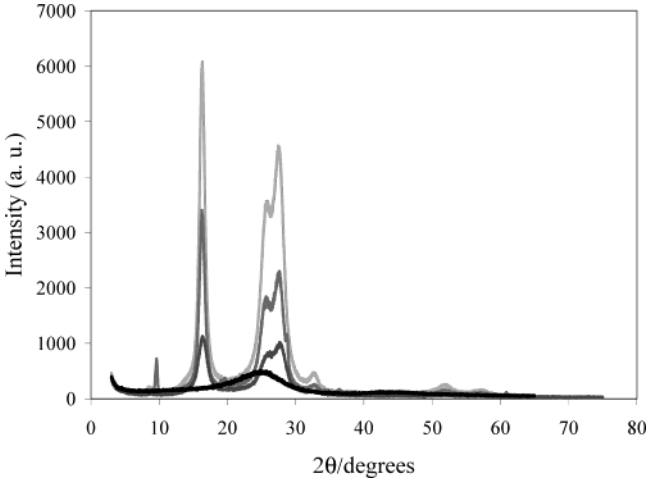

Figure 4. Equatorial X-ray diffractograms of fresh Zylon AS fiber (dark grey) and fibers heat-treated to 773 K (grey), 883 K (pale grey), and 1073 K (black).

Table 2. Average Crystal Size (nm) of PBO Fibers

	lateral (200)	axial (005)
AS	5.6	7.5
AS HT 773	7.8	
AS HT 883	8.7	
HM	9.2	8.2
HM HT 773	9.4	
HM HT 883	9.7	

fibers. The greatest increase takes place for AS fibers, approaching the values for HM fibers for the highest temperatures. Such behavior arises from the aforementioned fact that fresh HM fibers have already undergone a thermal treatment under tension during their manufacturing process whereas AS fibers have not.

At higher temperatures, the polymeric X-ray diffractograms give way to patterns typical of disorganized carbonaceous materials (see Figure 4), and consist of two wide diffraction bands around 25° and 45°, corresponding respectively to (002) and (10) planes of a pseudographitic crystalline structure. The interlayer spacing, d_{002}, and the apparent crystal size along the *c* axis, L_c, were obtained from the (002) peak and are, respectively, 0.362 and 1.12 nm.

Atomic Force and Scanning Tunneling Microscopy Investigarions. Figure 5 shows typical tapping mode AFM images of the fresh and heat-treated AS PBO samples. Because the degradation behavior of the HM sample was found to be totally parallel to that of the AS polymer, and the increase in crystallinity observed before degradation is more appreciable in the AS sample, results are presented only for the latter, which is considered as a more general case. First, it is noted that the starting fiber displays a network of oriented nanofibrils, as can be seen in Figure 5a and, with more detail, in Figure 5b. The nanofibrils are normally between 10 and 25 nm wide and several tens of nm long, and lie parallel to the fiber axis direction (from top to bottom in all the images presented in this work). Such fibrillar morphology has been previously observed by AFM on other rigid-rod polymers,[29] and is interpreted to reflect the molecular conformation of the polymer, i.e., the orientation of the rigid-rod PBO

(29) Montes-Morán, M. A.; Paredes, J. I.; Martínez-Alonso, A.; Tascón, J. M. D. *Macromolecules* **2002**, *35*, 5085.

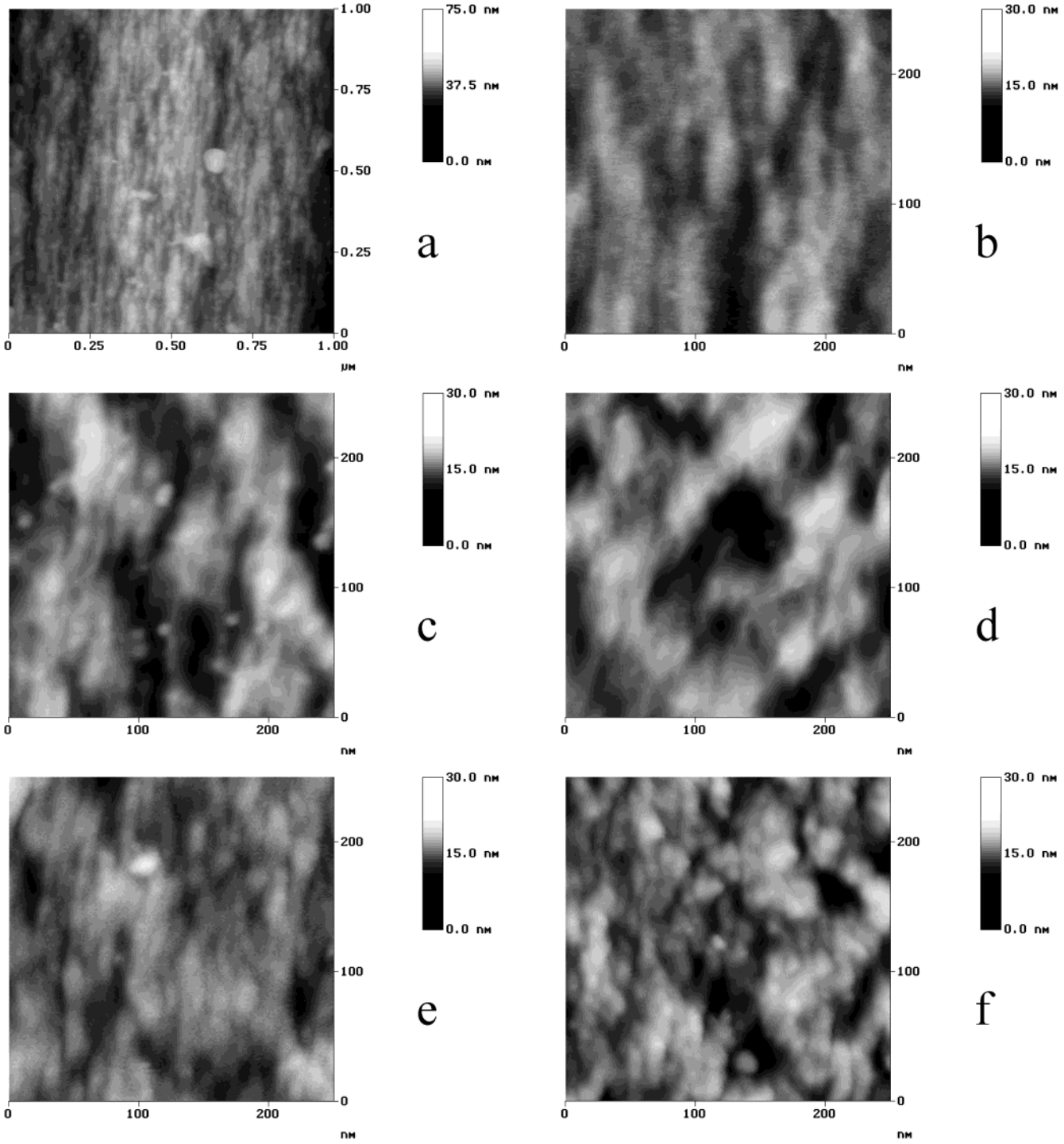

Figure 5. AFM images showing the nanometer-scale morphology of fresh PBO (a and b) and of PBO samples heat-treated to 933 (c), 983 (d), 993 (e), and 1073 K (f).

macromolecules in the direction of the fiber axis. However, because the average lateral dimension of single PBO crystallites in AS fibers (~6 nm from Table 2) is considerably smaller than the values reported here by AFM for the nanofibril dimensions, we conclude that the latter represent in most cases ensembles of several crystallites rather than individual ones. Single crystallites of just a few nm are difficult to resolve by this technique when the surface under consideration is not perfectly flat, as is the case with the present samples. Figure 5c to 5f shows representative images of the PBO fiber surface following heat treatments to different significant temperatures: 933 (c), 983 (d), 993 (e), and 1073 K (f). It can be appreciated that the 933 K sample (Figure 5c) has undergone subtle changes when compared with the starting polymeric material (Figure 5b). Although an arrangement of oriented nanofibrils is again the most prominent morphological feature of this heat-treated sample, the nanofibrils in this case tend to appear slightly thinner (typically ranging from 5 to 15 nm) and more clearly defined than those in the fresh PBO fiber. Because all the images were obtained under the same tapping mode AFM operating conditions and the morphological differences between the fresh and 933 K samples were reproducibly observed, the origin of such differences as arising from AFM imaging artifacts

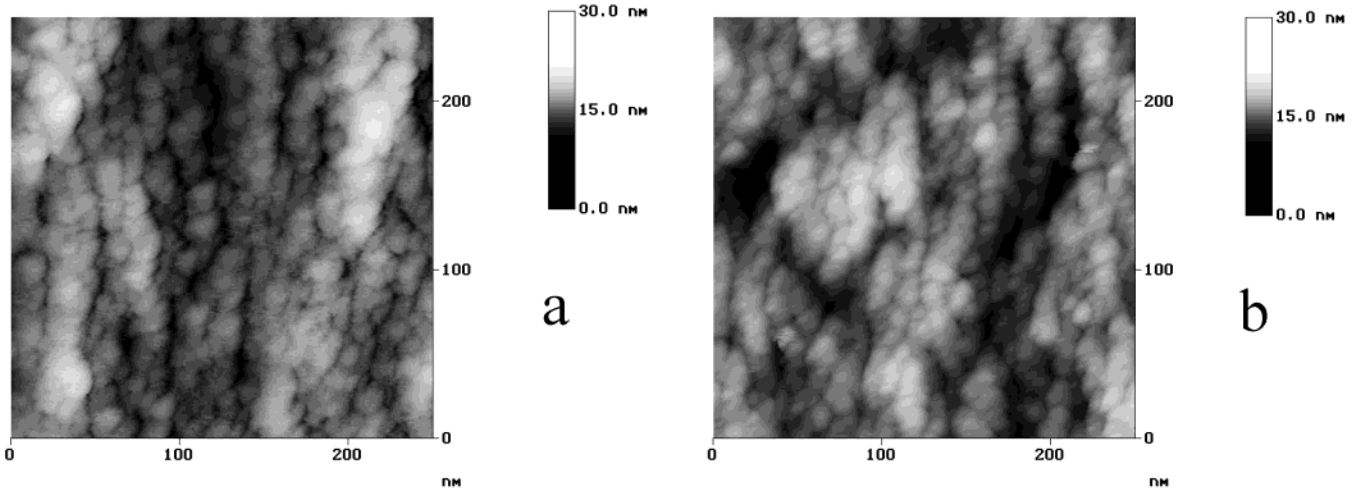

Figure 6. Typical STM images of PBO pyrolyzed at 993 (a), and 1073 K (b).

can be ruled out. Then, it can be inferred that they arise from structural changes undergone by the polymer during this heat treatment. Next, considering that the critical phase in the pyrolytic degradation of the PBO fiber occurs, as mentioned previously, in a narrow heat treatment temperature range (983−993 K), images are presented for these two close temperatures: 983 K (Figure 5d), corresponding to the onset of the critical phase, and 993 K (Figure 5e), for which the transformation has just taken place. In the former case, the polymer often presented a morphology similar to that of the 933 K sample, as shown in Figure 5d. Nevertheless, it should be mentioned that a certain degree of morphological variability was noted as well, in such a way that some areas of the sample surface were more comparable to the 993 K sample (Figure 5e) than they were to the 933 K one. Such heterogeneity was only noticed for this particular temperature, as the rest of the samples appeared highly homogeneous. In turn, this would suggest a relative lack of uniformity in the polymer degradation, which is not surprising if we take into account the fact that the decomposition mainly occurs in one rapid step around the mentioned temperatures. Upon pyrolysis at 993 K, the morphological homogeneity is recovered and the surface appears decorated with more or less rounded or slightly elongated platelets having lateral dimensions typically in the 5 to 20 nm range (Figure 5e). It is likewise apparent that the platelets are in many cases lined up along the fiber axis direction. Finally, when the heat treatment is carried out at 1073 K, the platelets (also between 5 and 20 nm wide) become more clearly the dominant morphological feature of the sample (Figure 5f). Although perhaps not so evident in this particular image, it should be mentioned that at 1073 K the alignment of platelets along the fiber axis was also usually observed.

Additional evidence of the changes undergone by the polymer and the structure of the final pyrolyzed samples was gathered by STM. First, it should be noted that below thermal treatment at 993 K (e.g., at 983 K) the samples lacked enough conductivity for STM imaging to be feasible, as no detectable tunneling current could be established and the STM tips crashed onto the samples. On the other hand, at 993 K STM imaging could already be achieved. The marked change in conductivity within this particular heat treatment temperature interval is consistent with the previous observations and further strengthens the idea that the key structural change in the PBO degradation process takes place between 983 and 993 K. Figure 6 shows typical STM images of the PBO samples pyrolyzed at 993 (a) and 1073 (b) K. In general terms, the images are consistent with their AFM counterparts (Figure 5e and f). However, as expected due to differences in resolution capabilities between AFM and STM, the platelets characteristic of these two samples are somewhat better resolved with the latter technique. Also particularly obvious in the STM images of both samples is the tendency of the platelets toward appearing aligned along the fiber axis direction, in a way that strongly mimics the nanofibrilar morphology of the PBO polymer prior to its main pyrolytic degradation at ∼983−993 K. Therefore, we conclude that the final carbonized material retains to some extent a memory of the original polymeric structure.

Discussion

On the basis of the previous results, several remarks regarding the thermal degradation process of PBO can be made.

(i) The first observable change undergone by the polymer takes place at a temperature bracket approximately between 800 and 933 K, as evidenced by an exothermal effect in the DTA curve. Such change does not involve either a mass loss of the material or a chemical change detected in the infrared spectra, excepting a decrease in the end groups (compare Figure 2a and b) which would suggest a lengthening of the polymeric chains. Furthermore, during this stage the sample experiences subtle morphological changes (Figure 5c), which again support the idea that some kind of structural rearrangement has occurred. Now, in principle, the exothermal process can be related to an enhancement in crystallinity of the polymer lattice. As a matter of fact, it was verified by X-ray diffraction (Table 2) that the mean apparent crystallite size in the present AS samples is noticeably enlarged upon heat treatments at temperatures in the mentioned range. In turn, this is consistent with previous transmission electron microscopy studies on PBO[3] and indicates that such a stage (i.e., between 800 and 933 K) in the

transformation process does not correspond to the genuine degradation but to a further structural stabilization of the polymer.

(ii) The pyrolytic decomposition of PBO takes place basically in a single step in a temperature range approximately from 933 to 1050 K and mainly involves two processes: (a) opening of the oxazole heterocycles, which is concurrent with an endothermal effect centered at 945 K in the DTA curve (Figure 1), and whereby the polymer could be transformed into a kind of polyaramide, as the infrared spectra suggest (Figure 2c and d); and (b) homolytic breaking of the polymeric backbone to yield nitriles (Figure 2e−h), coincident with an endothermal effect centered at 993 K in the DTA curve (Figure 1). As mentioned previously, nitriles have been observed by other authors as evolved products during the decomposition of PBO.[14] Process (b) would be analogous to that of polyaramides at high temperatures,[19,28] namely the homolytic breaking of the amide bond. Moreover, it could be established that the most drastic change in the material was confined to a very narrow temperature window between 983 and 993 K. During this temperature interval any trace of the polymer is lost and the carbonaceous residue takes over. This was evidenced in the infrared spectra obtained in this work (Figure 2f −h) by the thorough substitution of the polymer peaks for wide bands typical of carbonized materials,[19,28] and also in the marked change from a nonconducting material (typical of polymers) to a conducting one (as expected from a carbon material) which was observed by STM within this particular temperature range. Concerning the platelet morphology detected by STM/AFM, which develops at 993 K (Figures 3e and 4a) and is retained in the final fibrous residue (Figures 3f and 4b), we note that it is typical of carbonized polymers, such as polyimide[30] or polyaramides.[19] However, in the present case of carbonized PBO the platelets tended to appear aligned along the fiber axis direction, thus retaining part of the anisotropy characteristic of the starting polymer, whereas for other polymers which originally display a similar anisotropic, nanofibrillar morphology, such as poly(*m*-phenylene isophthalamide), the disposition of the platelets in the final carbonized residue became completely isotropic.[19] In our opinion, the origin of such differences should be sought in the mechanisms of the degradation of both polymers, which present significant differences. In the latter case the degradation takes place gradually in several different steps, and begins with the rupture of the hydrogen bonds between the polyaramide chains, which are free to rearrange and curl up in a disorganized way.[19] Thus, by the time the covalent bonds within the polymer chains start to cleave in a process that finally leads to the carbon residue, the material already displays a considerably isotropic morphology. Therefore, no memory of the initial anisotropy is preserved in this polymer. By contrast, the processes undegone by PBO prior to its pyrolytic decomposition above 933 K lead to an increase in crystallinity, implying that the anisotropy is maintained or enhanced a little. The AFM images presented here showed evidence of this effect (Figure 5). As a result, above 933 K the PBO chains break up while retaining their stretched arrangement and, consequently, the carbonized residue retains to some extent a memory of the original polymeric structure in the form of aligned (rather than isotropically disposed) platelets.

(30) Nysten, B.; Roux, J.-C.; Flandrois, S.; Daulan, C.; Saadaoui, H. *Phys. Rev. B* **1993**, *48*, 12527.

Conclusions

Infrared spectroscopy and scanning probe microscopies have provided useful direct information on the thermal degradation of PBO, which was not previously available. The decomposition basically takes place in a single step at temperatures above 933 K up to the development of the final fibrous carbon at 1050 K, which stresses the extremely high thermal stability of the material. Below this range of temperatures, the polymer not only retains its original conformation but is further stabilized through an enhancement in crystallinity. Such behavior is markedly different from that of polymers that possess intermolecular hydrogen bond networks, and leads to the preservation of a certain degree of anisotropy in the final carbonaceous residue. The direct study of the solid residue allowed us to detect the formation of polyaramides as intermediates in the decomposition process, which subsequently degrade in the manner expected for such molecules (i.e., homolytic breaking of the amide bonds to yield nitriles).

Acknowledgment. We thank Toyobo (Japan) for supplying the PBO samples. Grateful recognition of support given by the 3rd PRI of Asturias for this research (Project PB-EXP01-06) is made. We also acknowledge a pre-doctoral fellowship from the Spanish Ministry of Education awarded to S.V.-R.

CM034336U